Astron. Astrophys. 344, 923–929 (1999)

ASTRONOMY AND ASTROPHYSICS

A strong magnetic field in the disk of MWC 349

C. Thum and D. Morris

Institut de Radio Astronomie Millimétrique, Grenoble, France

Received 3 July 1998 / Accepted 4 January 1999

Abstract. Using Zeeman observations of the H30α recombination line maser transition at 1.3 mm we have detected a magnetic field which is associated with the corona of the circumstellar disk of MWC 349. At a radial distance of 40 a.u., where the H30α maser is located, the line–of–sight component of the field is approximately parallel to the plane of this edge–on disk, and its average strength is 22 mG. The corresponding magnetic energy density is $\sim$ 70% of the thermal energy density of the plasma where the maser emission originates, very likely making the detected field dynamically important. Spectral fine structure of the detected Zeeman pattern suggests that the field may have a strong radial component, although other models for the field configurations are possible. The strength of the field at such a large distance from the star makes it unlikely that the field is of stellar origin. We suggest that it is generated by a local disk dynamo.

Key words: magnetic fields – masers – polarization – stars: circumstellar matter – stars: individual: MWC 349 – radio lines: stars

1. Introduction

Magnetic fields are thought to play a critical role in several stages of the evolution of young steller objects. The field may constitute a threshold which regulates the gravitational collapse of cloud cores. After collapse has started and a disk is formed, the field may be essential for channelling some of the accreting matter into an outflow. As a central requisite of the accretion process, magnetic field induced turbulence may provide the necessary viscosity for disk accretion to work.

While magnetic fields are now detected in ever denser clouds and cloud cores (Fiebig & Güsten 1989), observational evidence for fields in disks is still indirect and only qualitative. Many T Tau stars may have strong stellar fields as suggested by their star spot activity (Bouvier et al. 1993), by their X–ray flaring (Preibisch et al. 1993), or by their non–thermal radio spectra (André 1996). In some cases, these fields may be sufficiently extended to affect an eventual inner disk. In only one young star, TAP35, has the stellar field been measured directly (Bouvier et al. 1993), and a field strength of $\sim 1\,kG$ was found from the Zeeman broadening of optical lines.

We have observed the peculiar emission line star MWC 349, most consistently interpreted as a massive young stellar object (Hamann & Simon 1986; Thum & Martín–Pintado 1994; Hollenbach et al. 1994). This has led to the first quantitative measurement of the magnetic field in the *disk* of any young star. We observed the Zeeman effect of the masing hydrogen recombination line H30α near 232 GHz. This transition originates in the very dense ionized corona dynamically associated with the neutral disk (Planesas et al. 1992). The two bright and narrow maser spikes permit a sensitive determination of the line–of–sight component of the magnetic field along two tangential lines of sight through the disk corona at radial distances of about 40 a.u. from the star. Since the disk is seen nearly edge–on, these lines of sight measure the field components almost parallel to the plane of the disk.

The presence of a magnetic field in the disk of MWC 349 was inferred before from spectropolarimetric observations at 10 μm (Aitken et al. 1990). The linear polarization found by these authors was interpreted as due to alignment of dust grains in the circumstellar disk by a magnetic field of estimated strength > 10mG and oriented perpendicular to the disk. Linear polarization was detected previously at optical wavelengths (Elvius 1974; Zickgraf and Schulte–Ladbeck 1989; Yudin 1996), but it may be attributed to scattering processes and thus testify for the flattened dust distribution rather than for a circumstellar magnetic field.

2. Observations

The Zeeman observations were made during the period 23–28 of June 1996 at the IRAM 30m telescope on Pico Veleta near Granada, Spain. We used one of the Observatory's standard 1.3mm SIS receivers together with a 512 channel filter spectrometer and a 2024 channel autocorrelator backend. The autocorrelator was operated in a split mode where the two halves covered 70 MHz bandwidth each, centered on the blue and red spikes, respectively, of the observed transition (H30α at 231.900 GHz). Spectral resolution was thus 80 kHz (0.10 km s^{-1}) with the autocorrelator and 1 MHz (1.3 km s^{-1}) with the filter spectrometer. The receiver, tuned for single side band, had a noise temperature of about 170 K, and typical sys-

Send offprint requests to: C. Thum

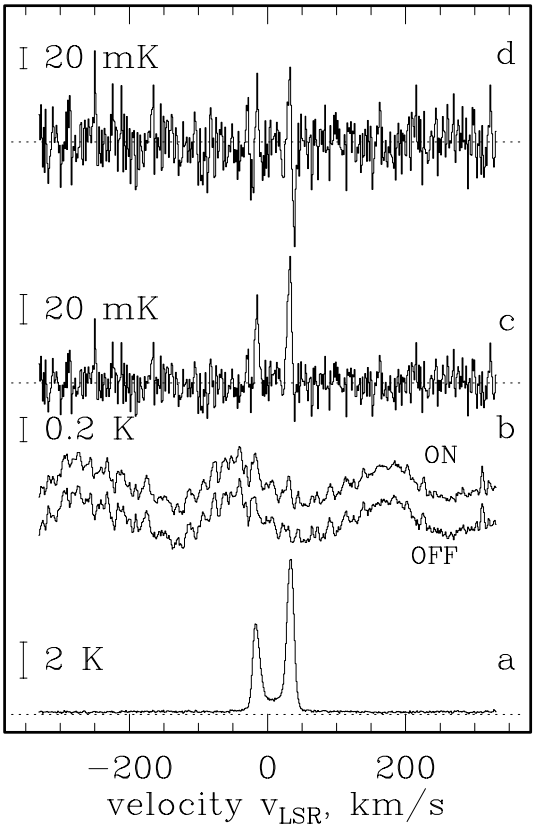

Fig. 1. Observations of the H30α transition in MWC 349 obtained on 24 June 1996. The spectral resolution is 1.0 MHz (1.3 km s^{-1}), intensities are in units of antenna temperature. The horizontal dashed lines mark zero intensity. The lowermost curve (a) shows the total power spectrum (Stokes I), integration time 4 min. Frames b–d show polarization switched (RHC – LHC) spectra of total integration time 40 min. In (b) the individual V–spectra observed ON and OFF source are displaced by ± 0.1 K for clarity, and their difference is given in (c). Correction for gain imbalance of 0.88% (slightly more than average, see Sect. 3.1) gives the final V–spectrum (d) for this particular observing sequence.

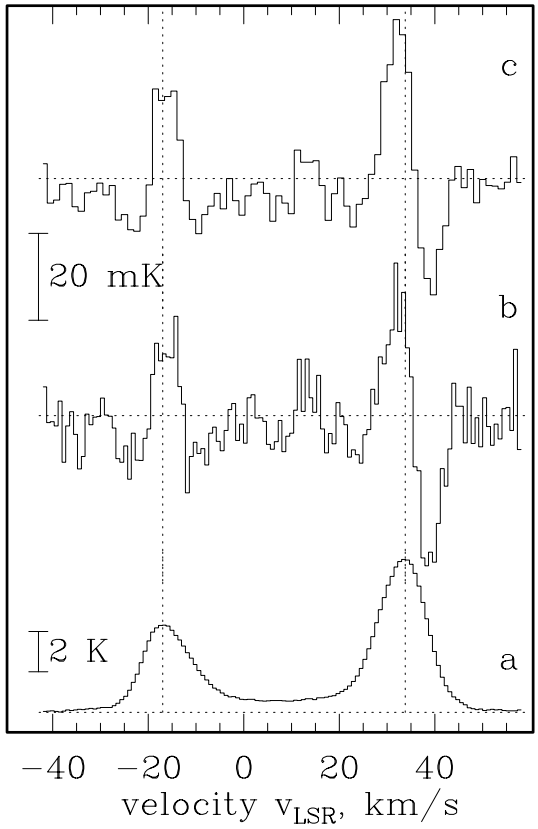

Fig. 2. Zeeman observations of the H30α transition in MWC 349, obtained with an autocorrelator backend and smoothed to a resolution of 0.7 km s^{-1}. All data obtained during 23–28 June 1996 have been averaged, representing 245 min of polarization–switched spectra. The three subframes show: (a) the total power spectrum (Stokes I), (b) the V–spectrum (RHC–LHC), corrected for instrumental polarization, (c) same as (b), but observed with the filter bank at a spectral resolution 1.3 km s^{-1}. Vertical dotted lines mark the maxima of the total power maser spikes.

tem temperatures of 600 K were obtained. The telescope beam has a full width at half power of $12''$.

For the polarization observations a quarter–wave plate designed (Lamb 1994) and manufactured by IRAM was introduced into the convergent beam between the receiver and the telescope's Nasmyth mirror, at a distance of 810 cm from the receiver. Using the same mount and control electronics as in a previous polarization experiment (Crutcher et al. 1996) the plate was switched between $\pm 45°$(angle between grooves and the vertical), thus converting the receiver's vertical linear polarization into right–hand (RHC) and left–hand circular (LHC) polarization. The data acquisition program calculated the difference between these RHC and LHC phases which is the desired spectrum of the Stokes V parameter. We switched the plate with a period of 4 sec and a duty cycle of about 80%. The transients were flagged and subsequently ignored by the acquisition program.

In a typical observing sequence we first observed the total power spectrum (Stokes–I) for a few minutes. We then obtained a one hour integration of about 15 cycles of polarization–switched spectra. Each such cycle consisted of four 30 sec integrations of RHC–LHC spectra, two of which were obtained on–source and the other two at off–source positions located symmetrically in azimuth at $30''$ away from the source. Subtraction of the OFF from the ON spectrum turned out to be very efficient in removing the baseline ripple generated by introduction of the quarter–wave plate. The resultant ON-OFF spectra were free of any ripple down to the level of the rms noise, and consequently there was no need to remove baselines, other than linear, from the ON–OFF spectra. We show in Fig. 1 the spectra obtained with the 1 MHz spectrometer in one such observing sequence.

Altogether we have obtained six such observing sequences, totaling 245 min of V–spectra and 80 min of I–spectra. Their average is shown in Fig. 2. The higher spectral resolution of the autocorrelator spectra did not reveal any spectral structure

finer than that visible already on the 1 MHz spectra. A smoothed correlator spectrum is included in Fig. 2.

3. Results

In all ON–OFF V–spectra of the six observing sequences we detect two positive features at the radial velocities of the blue and red maser spikes of the I–spectrum. No polarization features are seen outside these velocities. The two circular polarization features are clearly detected with 10 to 20σ in any one of the observing sequences, and their peak intensity relative to the total power spikes is about 1%, nearly the same in all six observing sequences. These features cannot be fully due to instrumental polarization, since their spectral shape is different from their I-spectrum counterparts. On the other hand, the detected features cannot be fully due to the Zeeman effect either, since they lack its characteristic S–shaped signature. Below we argue that they are in fact due to a combination of the two mechanisms, with similar contributions from each of them. A detailed analysis of instrumental effects is therefore in order before the magnitude of the Zeeman effect can be derived.

3.1. Instrumental effects

The principal instrumental effects complicating Zeeman radio observations are *(i)* the beam squint, *(ii)* leakage of linear polarization, and *(iii)* gain imbalance (Heiles 1987a; Fiebig and Güsten 1989; Crutcher et al. 1996). Beam squint, a small misalignment between the RHC and LHC telescope beams, can mimic a Zeeman feature when an extended source with some velocity gradient is observed. In our case, however, the maser spikes originate at locations only $0.065''$ apart (Planesas et al. 1992). Our source must therefore be considered pointlike with respect to the beamwidth of $12''$, and beam squint can be neglected.

Leakage of linear polarization can occur if the relative phase lag introduced by the quarter–wave plate between its two orientations is different from 90°. Measurement of the optical performance of our quarter–wave plate with a network analyser showed that the phase lag between beams polarized parallel and perpendicular to the grooves is only 87° at our observing frequency. The linearly polarized beam from the receiver is therefore not converted into a 100% circularly polarized beam, but contains a small linear component of magnitude 2.5 percent, implying that a $p_L = 100\%$ source gives a false V–signal of $p_C = 2.5\%$. The H30α transition for which an upper limit of $p_L = 15\%$ was obtained (Thum et al. 1992) may therefore introduce a false p_C of less than 0.4%. In fact, any linear polarization of H30α is probably much smaller than the 15% upper limit due to the strong Faraday rotation expected in the maser emission region (~ 2 rad/mG per unit gain length).

These considerations then suggest that the strongest instrumental effect in our case is a gain imbalance ΔG between the RHC and LHC beams. We estimated its magnitude at our observing frequency from the observations of MWC 349 itself, the strongest H30α source available. The method consists in subtracting from the ON–OFF V–spectrum a fraction ΔG of the I–spectrum so that the residual V–spectrum has zero power integrated over a certain bandwidth, i.e. the residual RHC and LHC polarization features are equally strong. In the simple case where the line emission region is threaded by a constant magnetic field our method and that used by Crutcher et al. (1996) are equivalent. Using bands of different width centered on the B and R spike respectively, or using the full bandwidth we derive

$$\Delta G = 0.71 \pm 0.12\%$$

The error describes the scatter for the different observing sequences. It is a bit larger than expected from the errors of ΔG in the individual sequences, probably reflecting real changes of ΔG between some of the sequences. The residual V–spectrum, i.e. the ON–OFF V-spectrum minus $\Delta G\cdot$ I–spectrum, is then the true Stokes–V spectrum. It is shown in Fig. 1 for one observing sequence and in Fig. 2 for the full data set.

In an attempt to obtain independent evidence for the magnitude of ΔG, we observed the H30α transition from the presumably unpolarized HII–regions W3OH and K3–50A which are about 20 times weaker than MWC 349. We derive $\Delta G = 0.5 \pm 0.4\%$ for W3OH and a 3σ upper limit of $\Delta G < 2.5\%$ for K3–50A. We also observed the much stronger (44 K) thermal CO emission at 230.58 GHz in W51d. The V–spectrum is simply a scaled down version of the I–spectrum and, assuming that this source is unpolarized, we have derived a $\Delta G = 0.7 \pm 0.2\%$ at that frequency. All these auxiliary observations support quantitatively our identification of the instrumental polarization signal as due to a small gain imbalance of 0.7%. A gain difference of this order between the two phases can arise from minor variations of the quarter–wave plate's reflection loss across its surface, a slight asymmetry of the switching angle, or from telescope properties.

3.2. Average field strength

The V–spectrum corrected for instrumental effects is related to the line–of–sight component B_{los} of the magnetic field (see e.g. Fiebig & Güsten 1989; Nedoluha & Watson 1992)

$$\frac{\Delta V}{I_0} w = 4.00\, g\, B_{los} \qquad (1)$$

where ΔV is the full peak–to–peak amplitude of the V–spectrum, I_0 and w denote the maximum of the I–spectrum and its full width at half power. The Landé factor g of the transition is taken as 1.0 for H30α in atomic hydrogen (Rust 1967; Troland & Heiles 1977; Greve & Pauls 1980; Casini & Landi Degl'Innocenti 1994). Eq. 1 uses a gaussian decomposition for the I–spectrum (Table 1), a sufficiently accurate procedure in our case.

Due to the near edge–on orientation of the disk B_{los} corresponds to a field which is mainly parallel to the disk surface. The observed field is therefore the toroidal and/or radial component of the field in the disk corona at ~ 40 a.u. on both sides from the star. In this simplified analysis B_{los} is assumed constant in the line emitting region. The fields derived in Table 2 therefore

Table 1. Gaussian decomposition of the I–spectrum.

component	T_A^*, K	v_c, km s^{-1}	w, km s^{-1}	remark
blue	3.91±.01	-16.1±.1	11.4±.1	[a]
red	7.37±.02	33.2±.1	11.7±.1	[a]
broad	0.60±.01	4.9±.8	63.8±1.2	

[a] broad component removed.

Table 2. Average line–of–sight magnetic field, in milliGauss.

component	$\Delta V/I_0$	B_{los}
blue	$8.8 \cdot 10^{-3}$	19 ± 4
red	$1.02 \cdot 10^{-2}$	23 ± 2

represent *average* values along each of the two lines of sight sampled by the blue and red spikes.

The average field strengths obtained are the same, ~ 22 mG within measurement accuracy, for both spikes. The receding and approaching sides of the circumstellar disk have comparable line–of–sight magnetic fields despite their large (factor 2) asymmetry in total power.

3.3. A radial field component?

Inspection of the V–spectra in Fig. 2 shows that there are substantial departures from the classical S–shaped Zeeman pattern. In the more severe case of the blue spike, the Zeeman pattern is rather W–shaped, with *two* negative excursions of about equal strength. In the red spike, although the second negative excursion is weaker, the departure from a classical Zeeman pattern is shown clearly by the velocity offset of the pattern from the maximum of the I–spectrum (dashed vertical lines).

Such W–shaped Zeeman patterns can arise in a situation where B_{los} reverses sign along sections of the line of sight where the gas has a significant velocity gradient. The resulting Zeeman pattern can be visualised as a superposition of two ordinary Zeeman patterns of opposite sense. The presence of the velocity difference between the two regions of opposite field polarity introduces a relative shift of the two patterns, so that they avoid self–cancellation. The simplified case where the line of sight passes through two equally bright cloud regions whose B_{los} and velocity offset Δv are equally strong, but of opposite sign, gives then a result much like that observed for the blue spike. The normalized peak–to–peak amplitude $\Delta V/I_0$ of this W–shaped Zeeman pattern is given by

$$\Delta V/I_0 = 8.68 \frac{B_{los} \Delta v}{w^2} \qquad (2)$$

where Δv is in km s^{-1} and the other variables and units are as in Eq. 1 above. With $\Delta V/I_0$ from Table 2 we obtain $B_{los}\Delta v = 78$ mG km s^{-1} for the blue spike. With the average field of 22 mG a velocity difference of ~ 4 km s^{-1} would therefore explain the W–shaped Zeeman pattern. This difference is not unreasonably large in view of the observed line widths (Table 1), and might even be unavoidable if each line of sight samples a large or full cross section of the disk which rotates with ± 25 km s^{-1} at the radial distance of the H30α maser (Thum et al. 1992). The inferred Δv is also small with respect to the thermal velocities (7.3 km s^{-1} in a T_e = 6500 K plasma), maintaining velocity coherence along the maser propagation path. We note that velocity coherence can probably be maintained across most of the slowly rotating disk (Ponomarev et al. 1994).

The important result of these considerations is that B_{los} needs to reverse sign along each of the two lines–of–sight sampled by the blue and red spikes. This can happen if the magnetic field has a *radial* component. The projection onto the line of sight of a purely toroidal field would not change sign, and would therefore not generate the observed W–shaped pattern.

4. Discussion

At radio frequencies the Zeeman effect has been detected in a variety of transitions, both atomic and molecular, from many sources (see e.g. Crutcher et al. 1996 and references therein; Crutcher et al. 1994; Heiles 1987b). Here we presented evidence for the first time of the Zeeman effect in a radio recombination line. Several attempts were made in the past using hydrogen and carbon recombination lines at cm–wavelengths (Troland & Heiles 1977; Harwit et al. 1979; Silvergate 1984), yielding upper limits of the order of 1 mG. Our detection of a much stronger field (Sect. 3.2) in the dense corona of the massive disk around MWC 349 uses the Zeeman effect in a new astronomical and physical context.

While the new astronomical context arises from the location of the field in a circumstellar disk and is being dealt with in Sects. 4.2 to 4.4, the new physical aspect concerns the detection of Zeeman splitting from an atomic transition, H30α, where the spontaneous transition rate is 160 s^{-1}. This is up to 10^9 times higher than in the transitions where radio Zeeman splitting was detected in the past (SiO, H_2O, OH, HI).

4.1. Maser propagation effects

In interpreting the observed Zeeman patterns we so far have ignored possible effects of maser propagation. These can strongly affect the polarization characteristics of the emergent radiation (Goldreich et al. 1973; Elitzur 1996) and can even create Zeeman–like patterns in the complete absence of a magnetic field (Nedoluha & Watson 1994). The nature and magnitude of the effects depend on a range of critical parameters, notably the degree of saturation, the relative size of line width w and magnetic splitting $g\Omega$, the stimulated emission rate R, and the degree of isotropy of the maser pump. Since a quantitative theory of the recombination line maser does not exist yet, we discuss its expected polarization properties by comparing with other better investigated astrophysical masers whose critical parameters may be close to those of the recombination line maser.

The largest errors in deriving magnetic field strengths from the observed "Zeeman pattern" are apparently made in the case of SiO masers where observed fields may have to be revised

downward by factors up to 10^3. In these circumstellar masers which resemble the recombination line maser in both being saturated and having $g\Omega < w$, a fake Zeeman pattern can be generated by the "intensity dependent effect" in which a large linear polarization is converted into circular (Nedoluha & Watson 1994). In the recombination line maser, such large linear polarization is not seen (Sect. 3.1), nor is the likely reason for its existance in SiO masers, unisotropic pumping by stellar IR photons, expected to be valid for the recombination line maser.

The essential requirement for the "intensity dependent effect" is that the stimulated emission rate $R \sim g\Omega > \Gamma$ (the relaxation rate), implying a rather narrow tuning of these parameters. In the 22 GHz water vapour masers which resemble the recombination line maser in the same two aspects mentioned above, the intensity dependent effect does not operate, because of an unfavorably low stimulated emission rate $R < g\Omega$ (Nedoluha & Watson 1994). Consequently, magnetic field strengths in interstellar H_2O clumps derived from a straight–forward interpretation of the 22 GHz Zeeman pattern (Fiebig & Güsten 1989) were found to agree with rigorous calculations to better than a factor 2 (Nedoluha & Watson 1992). In the recombination line maser the essential requirement for the "intensity dependent effect" is also not satisfied, since Γ appears to be an order of magnitude larger than $g\Omega$ ($2\ 10^5\ s^{-1}$). The relaxation rate Γ is dominated by collisions out of the $n = 31$ level, and we obtain $\Gamma = 4\ 10^6\ s^{-1}$ for a density of $n_e = 3\ 10^7$ cm^{-3} (Sect. 4.2). Conditions for the "intensity dependent effect" are therefore not right in the recombination line maser, and we conclude that the straight forward interpretation of our Zeeman spectra is justified.

4.2. An equipartition field

The importance of a magnetic field in a given physical environment is usually assessed by comparing its corresponding magnetic energy density, $\frac{B^2}{8\pi}$, to u, the thermal energy density of the plasma in which the field is embedded. The physical parameters, T_e and n_e, of the plasma where the H30α recombination line maser is active, are known to good precision. The electron temperature T_e is determined from radio continuum studies (White & Becker 1985) and recombination line observations (Martín–Pintado et al. 1989) to be 6500 K with an error of no more than 1000 K. The electron density is determined (within a factor 3) as $n_e \sim 3\,10^7$cm^{-3} from the need to maintain population inversion at the level with $n = 30$ (Walmsley 1990). The uncertainty in n_e may be even smaller if the H30α maser operates under optimum conditions where its gain is highest (Strelnitski et al. 1996). The plasma energy density is therefore $u = 4\,10^{-5}$ erg cm^{-3} to within a factor 2. The equipartition field is then, with even better precision

$$B_{eq} = \sqrt{8\pi u} = 32 \text{ mG}$$

The observed average B_{los} (Table 2) is about 70% of B_{eq}, a remarkably close coincidence. We note that the true field strength, corrected for projection and dilution effects, may only be higher. This strongly suggests that the magnetic energy density of the field is comparable to the thermal energy density of the plasma in the maser propagation region, making the field dynamically important in the disk corona.

4.3. Left/right asymmetry

The red and blue components differ in total power intensity and it has been suggested that this may be due to slow radial motion of the ionized gas (Thum et al. 1994). The circularly polarized profiles show a certain overall similarlity in shape and after correction for the disparity of total power intensity, yield fields of comparable strength for the red and blue components (Table. 2). This suggests that the line of sight magnetic field has the same sense in both masing regions, or that the field is oppositely directed *and* the velocity gradient also reverses across the disk. However the red component has a more pronounced "S" shape. This difference in pattern shape between the two spikes suggests then that the red spike samples more of the toroidal field whereas the blue spike is more sensitive to the radial field. Such effects can be due to the slight tilt of the disk, $\sim 15^\circ \pm 5^\circ$ (Rodriguez and Bastian 1994), from the true edge–on configuration. Alternatively, the blue and red maser spikes may sample their respective lines of sight in systematically different ways.

In all this discussion it should be born in mind that the uncertainty in the calibration of the instrumental polarization is about 0.12%, so that small asymmetries of this order in the polarized line profile may be spurious.

4.4. Origin of the field

The H30α recombination line maser propagates along two lines of sight which are approximately parallel to the disk plane and are located roughly symmetrically at $R_{30\alpha} = 40$ a.u. from the central star. The kinematic coupling of the maser to the disk's rotation and the high electron density required for inversion suggest that the maser propagates close to the base of the ionized corona of the disk. We briefly discuss three possible scenarios for the origin of the magnetic field at these rather specific locations: *(i)* a large scale stellar field, *(ii)* a fossil interstellar field, and *(iii)* a field generated in situ by a local dynamo.

If the detected field of 22 mG is due to a normal stellar dipole field, it scales back to the stellar surface as $(R_{30\alpha}/R_*)^3$. Assuming a stellar radius $R_* = 7R_\odot$, characteristic of a massive star near the main sequence, we obtain $R_{30\alpha}/R_* \sim 10^3$, i.e. a magnetic field of $22\ 10^6$ G at the stellar surface. This implausibly high value suggests that the field falls off much less steeply than R^{-3} or that the detected field does not originate at all in the star. The more plausible R^{-1} dependence (Pelletier & Pudritz 1992) leads however to field strengths near the star which may be too low for magnetospheric accretion to occur (Camenzind 1990; Königl 1991).

More importantly, a stellar dipole field detectable at 40 a.u. from the star, would imply a very large and energetic magnetosphere. Ionized matter must be expected to be injected into the magnetosphere from the massive star and from the disk corona. However, neither the associated non–thermal radio emission

(Altenhoff et al. 1994) nor the expected X–ray emission (André 1996) are seen. We therefore discard a stellar origin of the observed field.

On the other hand, the observed field strength appears compatible with scenarios where the disk field originates by compression of a dense prestellar core. Taking average values for the 4 most compact cores listed by Myers and Goodman (1988) we get 4.5 mG for a 3000 a.u. sized core. If this average core evolves under constant mass to magnetic flux ratio, M/Φ, we predict ~ 150 mG for the approximately 300 A.U. sized disk of MWC349A, not too different from the the value implied by the observations. However, it is questionable whether the constant M/Φ evolution of prestellar cores can be extrapolated to the point when disk and star have formed. We must rather expect that virtually all of the magnetic flux is lost due to reconnection of field lines and ohmic dissipation during the final turbulent phases of massive star formation.

An interesting alternative which avoids the problems associated with a stellar or interstellar origin is the generation of the field in situ, either by a local disk dynamo (Stepinski 1995) or by magnetic instabilities (Tout and Pringle 1992). Both mechanisms may well be capable of generating magnetic fields of the strength and geometry reported here. We suggest that one of these local mechanisms is probably responsible for the magnetic field detected in the disk of MWC349A. Observations of the temporal and spatial coherence of the field may provide clues for discriminating between an origin of the magnetic field which is internal or external to the disk.

5. Conclusions

The surprisingly strong magnetic field which we detected in MWC 349 is the first such field reported for any circumstellar disk. The field is located near the base of the disk corona at about $R_{30\alpha} \sim 40$ a.u. from the star. In these regions of the disk corona the observed average line–of–sight field strength is ~ 22 mG. This is about 70 percent of the equipartition field B_{eq} – the field strength where the magnetic energy density equals the thermal energy density of the plasma in the maser propagation region. The true field strength must be higher than 22 mG when projection and dilution effects are taken into account. Thus the field is likely to be be important dynamically, possibly supporting the launching of the strong ionized wind from the disk (Hollenbach et al. 1994).

Our Zeeman observations measure the longitudinal component of the field B_{los}. Since the MWC 349 disk is oriented nearly edge–on, the detected field component is principally parallel to the disk. It is less clear what the relative contributions are to B_{los} from radial and toroidal components. We suggest that the red maser spike which is the stronger of the two spikes and which has a near–classical Zeeman feature, samples mainly the toroidal field. The Zeeman feature associated with the weaker blue spike departs strongly from the classical S–shape. We show that this shape portraits a sign reversal of the field along the propagation direction of the blue spike. This is evidence for a significant radial field component in the disk.

When combined with the field orthogonal to the disk, as inferred from the $10\,\mu$m polarimetry (Aitken et al. 1990), our observation of the parallel component indicates a complicated geometry for the magnetic field. In view of the non–negligible optical depth at $10\,\mu$m, both observations may refer to similar radial zones in the outer disk. The field may thus start out normal to the midplane of the disk where it is neutral and dusty, and then develop toroidal and radial components higher up in the corona where they are sampled by the H30α maser. But more complex geometries are certainly not excluded by the few existing observations.

Our detection of a rather strong field at a large distance (40 a.u.) from the star makes it unlikely that the field originates in the star. We argue that the non–thermal radio and the X–ray emisssion expected from the enormous magnetosphere are not seen. Since compression of a fossil interstellar field is also unlikely given the strong losses due to ohmic disspipation and field reconnection during the formation of the star/disk system, we propose that the observed field is generated in situ by some kind of disk dynamo.

Acknowledgements. We would like to thank the IRAM receiver group, notably J. Lamb, M. Carter, and F. Mattioco, for their support. G. Paubert helped with the operation of the quarter–wave plate and the calibration of the data. We also thank B. Lazareff for his interest in this work and for support. R. Pudritz and W.D. Watson are thanked for their very valuable comments on the theoretical interpretation of the observations.

References

Aitken D.K., Smith C.H., Roche P.F., Wright C.M., 1990, MNRAS 247 466
Altenhoff W.J., Thum C., Wendker H.J., 1994, A&A 281, 161
André Ph., 1996, ASP Conf. Ser. vol 93, 273
Basri G., Marey G.W., Valenti J.A., Bouvier J., 1992, ApJ 390, 622
Bouvier J., Cabrit S., Fernandez M., Martín E.L., Matthews J.M., 1993, A&A 272, 176
Camenzind M., 1990, Rev. Mod. Astron.3, 234
Casini R., Landi Degl'Innocenti E., 1994, A&A 291, 668
Crutcher R.M., Troland T.H., Lazareff B., Kazès I., 1996, ApJ 462, L79
Crutcher R.M., Mouschovias T., Troland T.H., Ciolek G.E., 1994, ApJ 427, 839
Elitzur M., 1996, ApJ 457, 415
Elvius A., 1974, A&A 34, 371
Fiebig D., Güsten R., 1989, A&A 214, 333
Goldreich P., Keeley D.D., Kwan J.Y., 1973, ApJ 179, 111
Greve A., Pauls T. 1980, A&A 82, 388
Hamann F., Simon M., 1986, ApJ 311, 909
Harwit M., Churchwell E., Walmsley M., 1979, Ap&SS 66, 487
Heiles C., 1987a, In: Hollenbach D.J., Thronson H.A. (eds.) Interstellar Processes. Reidel Publ. Co., p. 171
Heiles C., 1987b, In: Morfill G.E., Scholer M. (eds.) Physical Processes in Interstellar Clouds. Reidel Publ. Co., p. 429
Hollenbach D., Johnstone D., Lizano S., Shu F., 1994, ApJ 428, 654
Königl A., 1991, ApJ 370, L39
Lamb J., 1994, Analysis of quarter wave plate performance. IRAM Internal Note, 5 January 1994

Martín–Pintado J., Bachiller R., Thum C., Walmsley C.M., 1989, A&A 215, L13
Myers P.C., Goodman A.A., 1988, ApJ 326, L27
Nedoluha G.E., Watson W.D., 1992, ApJ 384, 185
Nedoluha G.E., Watson W.D., 1994, ApJ 423, 394
Pelletier G., Puditz R.E., 1992, ApJ 394, 117
Ponomarev V.O., Smith H.A., Strelnitski V.S., 1994, ApJ 424, 976
Planesas P., Martín–Pintado J., Serabyn E., 1992, ApJ 386, L23
Preibisch T., Zinnecker H., Schmitt J., 1993, A&A 279, L33
Rodriguez L.F., Bastian T.S., 1994, ApJ 428, 324
Rust D.M., 1967, ApJ 150, 313
Silvergate P.R., 1984, ApJ 279, 694
Stepinski T.F., 1995, Rev. Mex. Astron. Astrofis. Conf. Ser. 1, 267
Strelnitski V.S., Ponomarev V.O., Smith H.A., 1996, ApJ 470, 1118
Thum C., Martín–Pintado J., Bachiller R., 1992, A&A 256, 507
Thum C., Matthews H.E., Martín–Pintado J., et al., 1994, A&A 283, 582
Thum C., Martín–Pintado J., 1994, ASP Conf. Ser. 62, 265
Tout C.A., Pringle J.E., 1992, MNRAS 259, 604
Troland T.H., Heiles C., 1977, ApJ 214, 703
Walmsley C.M., 1990, A&AS 82, 201
White R.L., Becker R.H., 1985, ApJ 297, 677
Yudin R.V., 1996, A&A 312, 234
Zickgraf F.–J., Schulte–Ladbeck R.E., 1989, A&A 214, 274